

Triggering an eruptive flare by emerging flux in a solar active-region complex

Rohan E. Louis¹ · Bernhard Kliem^{2,3} · B. Ravindra⁴ · Georgios Chintzoglou³

Received 12 February 2015 / Accepted ...

© Springer ●●●

Abstract A flare and fast coronal mass ejection originated between solar active regions NOAA 11514 and 11515 on July 1, 2012 in response to flux emergence in front of the leading sunspot of the trailing region 11515. Analyzing the evolution of the photospheric magnetic flux and the coronal structure, we find that the flux emergence triggered the eruption by interaction with overlying flux in a non-standard way. The new flux neither had the opposite orientation nor a location near the polarity inversion line, which are favorable for strong reconnection with the arcade flux under which it emerged. Moreover, its flux content remained significantly smaller than that of the arcade ($\approx 40\%$). However, a loop system rooted in the trailing active region ran in part under the arcade between the active regions, passing over the site of flux emergence. The reconnection with the emerging flux, leading to a series of jet emissions into the loop system, caused a strong but confined rise of the loop system. This lifted the arcade between the two active regions, weakening its downward tension force and thus destabilizing the considerably sheared flux under the arcade. The complex event was also associated with supporting precursor activity in an enhanced network near the active regions, acting on the large-scale overlying flux, and with two simultaneous confined flares within the active regions.

Keywords: Flares, Dynamics; Sunspots, Magnetic Fields; Chromosphere, Active; Corona; Prominences, Active

1. Introduction

Eruptive solar flares arise from a disruption of the coronal magnetic field, which evolves into a coronal mass ejection (CME). In many cases a filament or promi-

¹ Leibniz-Institut für Astrophysik Potsdam (AIP), An der Sternwarte 16, 14482 Potsdam, Germany email: rlouis@aip.de

² Institut für Physik und Astronomie, Universität Potsdam, Karl-Liebknecht-Str. 24-25, 14476 Potsdam, Germany

³ School of Physics, Astronomy and Computational Sciences, George Mason University, Fairfax, VA 22030, USA

⁴ Indian Institute of Astrophysics, Koramangala, Bengaluru 560034, India

nence eruption is associated. The flare source region comprises highly sheared magnetic fields in the corona that overlie a photospheric polarity inversion line (PIL) (Martres *et al.*, 1968; Hagyard, Venkatakrishnan, and Smith, 1990; Wang, 2006). These locations inevitably show a filament channel in the chromosphere and often contain a filament or prominence in the corona above (Martin, 1998). It is widely (but not universally) accepted that a filament represents a weakly twisted magnetic flux rope holding the cool material (Mackay *et al.*, 2010). The formation and instability of a flux rope is a key element of storage-and-release eruption models (van Tend and Kuperus, 1978; Forbes and Priest, 1995; Amari *et al.*, 2003; Gibson and Fan, 2006; Mackay and van Ballegooijen, 2006; Kliem and Török, 2006).

Eruptions can be triggered through the emergence of flux as well as through flux cancellation. In the case of the former, the eruption occurs when newly emerged magnetic fields appear in a region of pre-existing flux, often in or in close proximity to a filament channel (e.g., Rust, 1972; Martin *et al.*, 1982; Demoulin *et al.*, 1993; Feynman and Martin, 1995; Li *et al.*, 2000; Saka-jiri *et al.*, 2004; Schrijver, 2009; Sun *et al.*, 2012). This can lead to the formation of a magnetic flux rope through bodily emergence (Low, 1996; Lites, 2005), by reconnection within an emerged magnetic arcade (Manchester *et al.*, 2004; Archontis and Hood, 2010), or by reconnection with the pre-existing flux (Kusano *et al.*, 2012). A number of variants for the triggering of eruptions by emerging flux have been proposed (see Section 5 for details). According to nearly all of them, the presence of pre-existing flux, orientated in a direction that facilitates reconnection with the emerging flux, is crucial to the eruption of the coronal flux rope (e.g., Chen and Shibata, 2000; Archontis and Török, 2008; Kusano *et al.*, 2012; Leake, Linton, and Antiochos, 2014). Otherwise, a specific, narrow range of locations (Xu, Fang, and Chen, 2008) or a large amount of emerging flux (Kaneko and Yokoyama, 2014) is required. Lin, Forbes, and Isenberg (2001) argued on general grounds that while the emergence of new flux can cause a loss of equilibrium, there is no simple, universal relation between the orientation of the emerging flux and the likelihood of an eruption, due to the complexity of the equilibrium surface in the multidimensional parameter space of the configuration.

Flux cancellation is also an important mechanism for triggering solar flares (Livi *et al.*, 1989; Sterling *et al.*, 2010; Green, Kliem, and Wallace, 2011; Savcheva *et al.*, 2012; Burtseva and Petrie, 2013). When canceling photospheric magnetic flux patches lie at the base of sheared coronal flux, then the cancellation is associated with magnetic reconnection low in the atmosphere. This gradually forms a filament channel in the photosphere and chromosphere and a flux rope above the PIL where the cancellation occurs (van Ballegooijen and Martens, 1989; Wang and Shi, 1993; Mackay and van Ballegooijen, 2006; Aulanier *et al.*, 2010; Amari *et al.*, 2011). The flux rope gradually rises as more flux is reconnected into it, implying a higher current flowing along the rope. When the rope becomes unstable and rises much faster, a vertical current sheet is formed underneath and becomes the site of fast “flare” reconnection (Lin and Forbes, 2000).

In this article we employ multiwavelength and dual-viewpoint observations to analyze an eruptive flare that originated between two active regions (ARs) that formed a quadrupolar active-region complex. Both the emergence of new

flux and flux cancellation occurred under the erupting middle flux lobe. The flux cancellation was weak, leaving the flux emergence as the primary candidate for the triggering of the eruption. However, the flux emergence did not correspond to any of the standard scenarios for such triggering: the direction and emergence site of the new flux were not favorable for strong reconnection with the pre-existing erupting flux, and its magnitude was only moderate. Additionally, the eruption was preceded by a complex sequence of events in the vicinity of the AR complex and accompanied by confined flares within the two ARs. The data analysis yields a suggestion for a non-standard triggering of the eruption by the emerging flux. We also discuss this eruption from a quadrupolar source region in relation to the breakout model (Lynch *et al.*, 2008; Karpen, Antiochos, and DeVore, 2012). A further eruptive flare in the region of flux emergence, following about 19 hr later and likely due to flux cancellation, was analyzed in Louis *et al.* (2014, hereafter referred to as Lo14).

2. Observations and data processing

We used full-disk solar observations from the Solar Dynamics Observatory (SDO; Pesnell, Thompson, and Chamberlin, 2012) that include data from the Helioseismic and Magnetic Imager (HMI, Schou *et al.*, 2012) and the Atmospheric Imaging Assembly (AIA, Lemen *et al.*, 2012) for the two ARs of interest. The HMI data set consists of $4k \times 4k$ -pixel images of continuum intensity and line-of-sight (LOS) magnetograms derived from the photospheric Fe I 617.3 nm line at a spatial sampling of $0.5'' \text{ pixel}^{-1}$. The HMI data were processed in a similar manner as described in Lo14. The AIA data consist of $4k \times 4k$ -pixel images with a spatial sampling of $0.6'' \text{ pixel}^{-1}$ in a range of UV and EUV bands. In particular, we have analyzed the bands including He II 304 Å, Fe IX 171 Å, Fe XII 193 Å, Fe XIV 211 Å, Fe XVI 335 Å, Fe XVIII 94 Å, Fe XXI 131 Å, and the continuum at 1700 Å. The observations span a duration of 28 hr starting on 2012 July 1 with a cadence of 12 sec for the AIA data and 45 sec for the HMI data.

We also used full-disk $H\alpha$ images from the Global Oscillations Network Group (GONG; Harvey *et al.*, 1996, 2011) recorded at Big Bear Solar Observatory. The $2k \times 2k$ images have a spatial sampling of about $1''$ with a cadence of 5 minutes and cover the passage of the eruptive flare.

Limb views of the event are provided by the SECCHI instrument package (Howard *et al.*, 2008) onboard the STEREO Behind spacecraft. We analyzed 195 and 304 Å data from the EUVI-B imager and data from the COR1-B coronagraph.

3. Source region

NOAA ARs 11514 and 11515 appear at the east limb on June 26, 2012 as young regions still in their emergence phase. By the beginning of July 1, their centers are located at S15E09 and S16E24, respectively. The leading AR 11514 is then already dispersing and spotless, while the following AR 11515 still develops

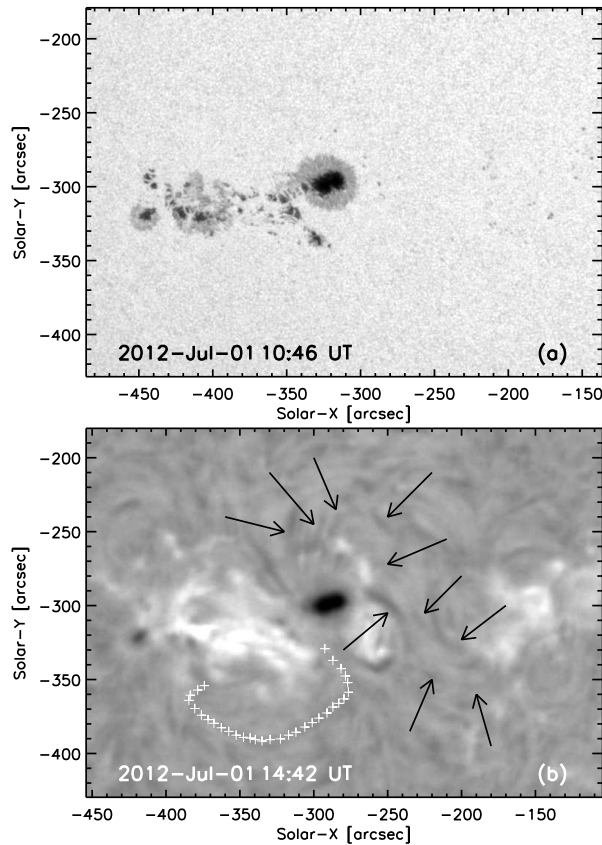


Figure 1. Overview images of the AR complex. (a) HMI continuum intensity; (b) GONG $H\alpha$ from Big Bear Solar Observatory ($H\alpha$ images from other observatories near the time of the other panels in Figures 1 and 2 are less sharp). Arrows in the bottom panel mark fibrils which indicate the forming filament channel involved in the eruption while the plus symbols indicate the overall alignment of $H\alpha$ fibrils south of AR 11515 with the loop system seen in the AIA 171 and 193 Å images (Figure 2(c-d)), similar to the absorbing material seen in He II 304 Å (Figure 2(b)). An animation of HMI continuum and magnetogram and AIA 171, 304, and 1700 Å images during July 1, 2012 is provided as online material.

strongly, with considerable rearrangements of its multiple spots. Both regions are essentially bipolar and follow Hale’s law, so that they jointly form a quadrupolar configuration. AR 11515 contains far more flux, amounting to 2.6×10^{22} Mx, while the total magnetic flux in AR 11514 is around 6.1×10^{21} Mx. Southwest of AR 11514, four areas of enhanced network with alternating polarity are located. Filaments have developed at all three resulting PILs, with the first two forming a joint, forward S-shaped filament, which becomes involved in the eruption studied here. The AR complex and adjacent enhanced network area are displayed at various wavelengths in Figures 1 and 2, and the accompanying animation shows their evolution during July 1. Their appearance in the AIA 211 and 335 Å bands is very similar to the appearance at 193 Å. It is also worth mentioning that AIA 211 and 193 Å images provide a weak suggestion for the existence of a magnetic

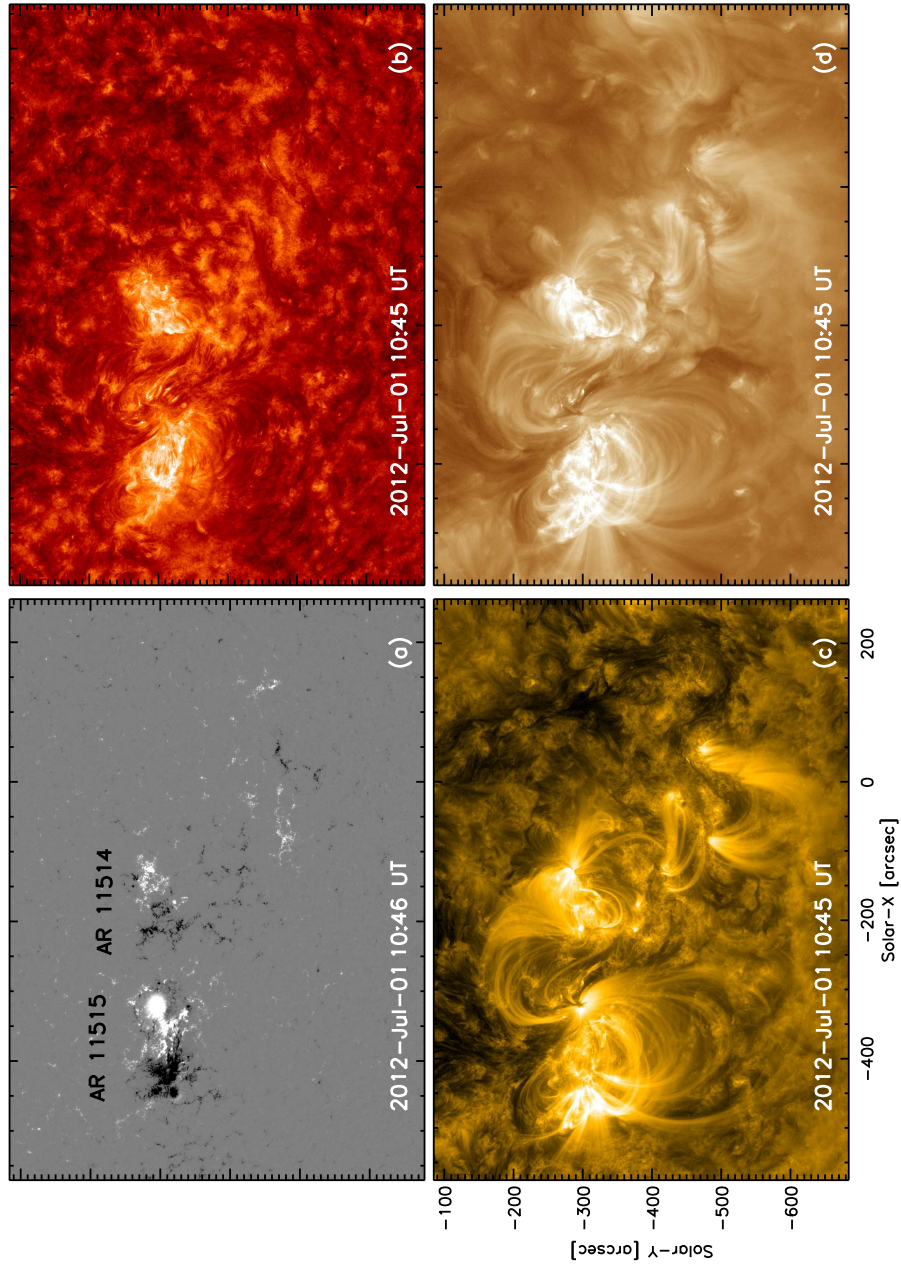


Figure 2. Continuation of Figure 1 showing (a) the HMI LOS magnetogram and the chromospheric and coronal structure in AIA images at (b) 304 Å, (c) 171 Å, and (d) 193 Å. The enhanced network area southwest of the AR complex, which contains the S-shaped filament centered at solar- $(x, y) = (0, -480)$, is included here.

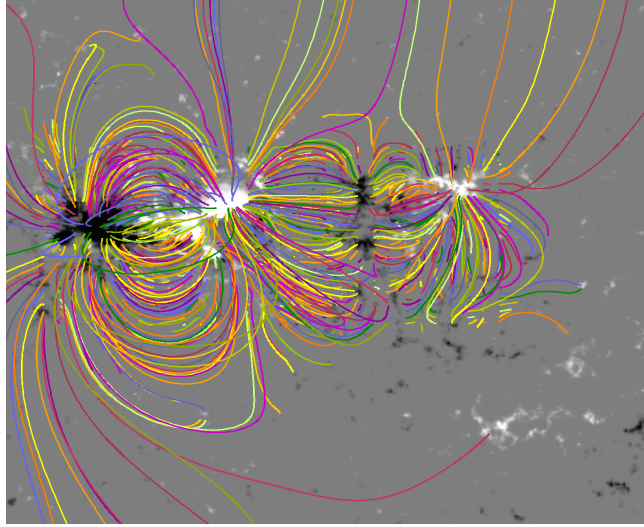


Figure 3. Field lines of a PFSS extrapolation using the HMI LOS magnetogram of ARs 11514 and 11515 and their environment at 15:24:45 UT patched into a synoptic full-Sun magnetogram. The field is computed using the method by Zhao and Hoeksema (1995) with 330 spherical harmonics and the source surface located at $2.5 R_{\odot}$. The grayscale of the magnetogram display is saturated at $|B|=500$ G.

connection between AR 11515 and AR 11513 located in the other hemisphere at N15E12. Both AR 11515 and 11513 are rather active during their disk passage, with much of temporally associated, possibly sympathetic activity occurring in the days around July 1–2.

Figure 3 shows field lines of a potential field source surface (PFSS) extrapolation of the AR complex immediately before the onset of the eruptive flare. One can clearly see that the two ARs are magnetically coupled: the excess positive flux in AR 11515, largely concentrated in the leading sunspot (LS), mostly connects to the excess negative flux in AR 11514, located in its trailing part. This yields the three-lobe magnetic configuration characteristic of a quadrupolar source region and agrees with the conclusion of Lo14 that the (later splitting) LS has strong magnetic connections with AR 11514. The PFSS extrapolation also indicates magnetic connections of both ARs with the enhanced network area southwest of AR 11514, and north-ward pointing field lines starting in the LS, which most likely connect to AR 11513, a region dominated by negative flux. High-reaching field lines are also rooted in both the leading positive polarity of AR 11514 and the trailing negative polarity of AR 11515. These may indicate the existence of an overarching fourth lobe of flux, as required by the breakout model, or open flux. While the PFSS extrapolation is not conclusive in this regard, the EUV observations described below (see Sections 4.1–4.2 and Figures 8 and 10) strongly suggest the existence of overarching flux, albeit with a different orientation. Moreover, the PFSS extrapolation indicates that the amount of overarching flux is considerably smaller than the flux in the three central lobes.

Beginning at about 05 UT on July 1 and continuing into the following day, new flux emerges in AR 11515 just in front (westward) of the LS, i.e. under

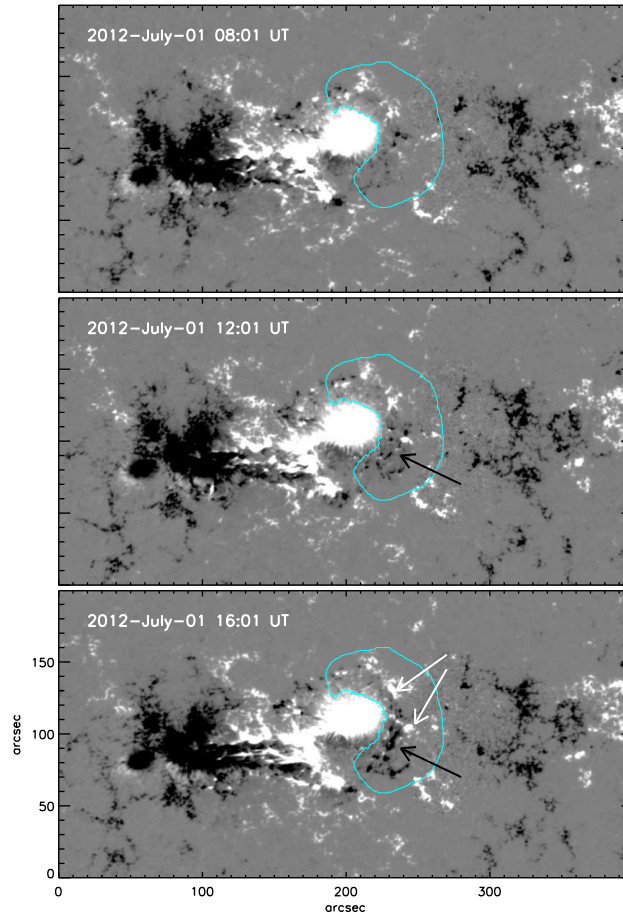


Figure 4. Emergence of new flux ahead of the LS in AR 11515. Mostly negative new flux can be seen, as indicated by the black arrows. Regions of increasing positive flux are marked by white arrows. The grayscale is saturated at $|B|=500$ G, except around the PIL between the ARs, where the flux has been enhanced by a factor of 4, to visualize the motion of weak negative flux in the trailing part of AR 11514 toward the PIL in the final hours before the eruption. The cyan contour outlines the region of emerging flux.

the middle magnetic lobe of the AR complex, near the left edge of the lobe (Figures 4 and 5). This is dominantly negative flux mixed with some small positive flux patches, thus forming a new PIL in front of the LS. It is difficult to discern with certainty where the corresponding positive flux emerges. Part of it must emerge within the preexisting scattered positive flux just outside the northwest periphery of the LS (marked by a white arrow). The amount of this flux clearly increases during the emergence of the negative flux ahead of the LS (Figure 5). Additionally, a moderate positive flux patch grows on the western side just in front of the emerging negative flux (marked by a second white arrow). It is possible, however, that part of the positive flux emerges in

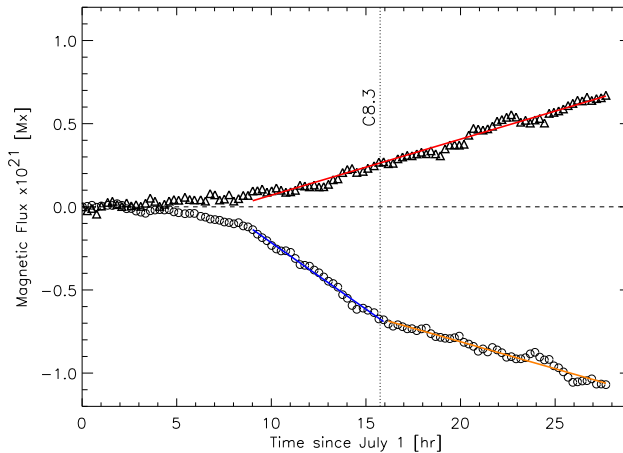


Figure 5. Temporal evolution of magnetic flux in the emergence area ahead of the LS (area enclosed by the cyan contour in Figure 4) in AR 11515 over the course of 2012 July 1. The triangles and circles correspond to positive and negative flux, respectively. The flux shown in the plot is relative to the initial flux at 00:00 UT. The blue and orange lines represent linear fits to the observed values, before and after the occurrence of the C8.3 flare.

the moat of the LS, where it is hard to detect. Any coronal field lines connecting the LS and the emerging negative flux must have a direction rather similar to the overlying flux of the middle lobe of the AR complex. However, the field lines connecting the two polarities within the emerging flux in front of the LS have a considerable north-south component, forming a small to moderate angle with the overlying flux. This allows for the occurrence of magnetic reconnection, although only with a moderate likelihood. The minor part of the emerging flux rooted in the moderate positive flux patch on the western edge of the emergence area is directed oppositely to the overlying flux; this flux has a high likelihood for reconnection to occur. The relative amount of emerged flux by the time of the eruptive flare is estimated from the measurement of negative flux in Figure 5 and from the amount of negative flux in the footpoint area of the middle flux lobe in the PFSS extrapolation to be $\sim 40\%$.

Another major development in AR 11515 is the splitting of its LS, which becomes apparent after the eruptive flare studied here and is analyzed in Lo14.

In the EUV (see Figure 2 and the corresponding animation), both active regions are bright throughout the observation, with the usual multitude of small-scale brightenings and changing coronal loops reflecting the ongoing evolution of the photospheric flux distribution. Additionally, the region of new flux emergence is bright and highly variable. Before the eruptive flare, there are fewer coronal loops between the ARs, and they are mostly fainter than the loops within the ARs. Many of the inter-region loops are also distinguished by their clear reverse-S shape, indicative of magnetic shear, and by their higher temperature, as they are more pronounced in the “warmer” AIA bands (193, 211, and 335 Å) than in the 171 Å band. The higher temperature is seen already before the new flux emergence and is therefore indicative of the dissipation of enhanced currents in the sheared field.

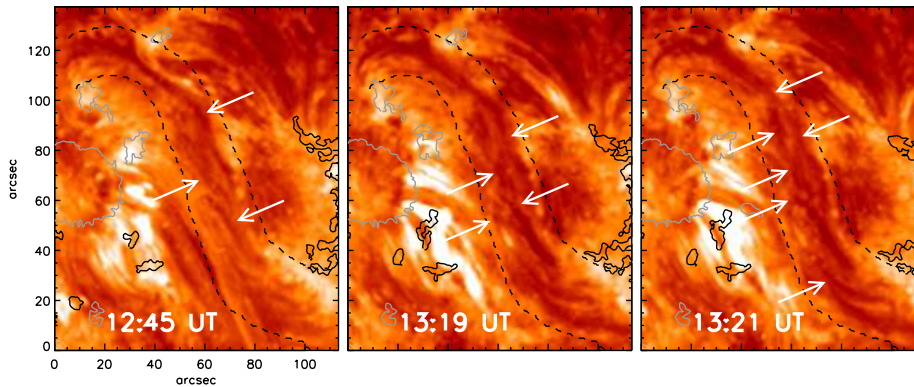


Figure 6. AIA 304 Å images of the forming filament channel between the two ARs showing instances of apparently crossing threads in the middle of the channel (indicated by the arrows). Dashed lines outline the filament channel. Gray (black) contours represent the LOS magnetic field of positive (negative) polarity.

The existence of considerable shear in the field between the ARs is also obvious from the strong alignment of the He II threads at the PIL of the central field lobe, shown in Figure 6. A filament channel, indicated in the figure, is obviously forming here; it extends with a reverse-S shape from the northern edge of the LS in AR 11515 to the southern edge of the trailing flux in AR 11514. Its shear is left-handed, consistent with the reverse-S shape of the overlying coronal loops. H α -absorbing material can be seen to be arranged along the forming filament channel in elongated patches (Figure 1). These patches are often changing in shape and position, with the trend to delineate the filament channel more completely by the end of the day.

Flows converging at the PIL are known to be essential for the formation of a filament channel (Martin, 1998). Since the photospheric field is weak in a broad strip around the PIL between the two ARs, an attempt to track magnetic features using the DAVE algorithm (Schuck, 2006) did not yield a reliable map of the photospheric flow field around the PIL. However, the sequence of HMI magnetograms unambiguously shows that the narrow strip of weak, mostly negative flux at the trailing edge of AR 11514 moves toward the PIL as a consequence of a strong expansion of the adjacent network cell from about 10 UT onwards (see Figure 4 and the AIA 1700 Å data included in the online movie).

The detailed arrangement of the threads in the forming filament channel is highly variable. Overall, they indicate a highly sheared, left-handed arcade at all times, but at a number of instances several threads display a crossing pattern that might indicate the formation of a flux rope (see examples in Figure 6). Since this pattern does not persist, the actual formation of a flux rope at this location remains unclear.

Absorbing (filament) material is also observed in the AIA 304 Å band (Figure 2(b)) in the heterogeneous structures extending up to $\sim 20^\circ$ south of AR 11515, which on a large scale are similar to the loops seen in the “warm” bands at 171 Å, 193 Å, and higher (Figure 2(c,d)). This cool material is also seen above the limb in EUVI-B 304 Å images, with variable shape (Figure 7(a)). The H α images

show an arrangement of the fibrils in this area in a large-scale loop pattern that resembles the structure in the AIA 304 Å band (some of them are indicated by crosses in Figure 1(b)).

Finally, we note that right-handed helicity is indicated for the filaments in the enhanced network southwest of AR 11514 by the orientation of the absorbing He II threads, the shape of the brightenings during their later activation (Section 4.1), and by the forward-S shape of the western filament.

4. Eruptive flare and associated pre- and post-flare activity

Both ARs 11515 and 11513 display frequent subflaring and flaring activity throughout the days around 2012 July 1, some of which might be sympathetic activity. Therefore, it is difficult to identify with certainty the initial element in a chain of events leading to the eruptive C-class (C8.3) flare in the AR complex formed by ARs 11514 and 11515, which peaks at 15:45 UT. These activities occur in different places in and around the AR complex, indicating a highly complex structure of the magnetic field, even if a possible connection to AR 11513 on the other hemisphere is not taken into account. Only part of this complexity can be inferred from the EUV images in the present article.

The basic sequence of events consists of (1) two relatively similar activations of the loop system containing filament material south of AR 11515, which remain confined, (2) the eruptive C8.3 flare and fast CME, which originate at the PIL between the two ARs but involve a complex pattern of bright ribbons and dimming areas scattered over the AR complex and the neighboring area of enhanced network flux containing two filaments, and (3) related confined flaring activities within the two ARs in the peak and decay phases of the eruptive flare.

4.1. Pre-flare filament activations

In the AIA data we count 19 episodes with single or multiple ejections of bright material from AR 11515 on July 1 before the eruptive flare; some of these were observed by EUVI-B as well. Initially, they all originate in the region's LS, but from 05 UT onward, the area of newly emerging flux (NEF) increasingly becomes the source of the jets. A double jet emission from the LS during 03:40–04 UT in both north and south directions deserves mentioning, as co-temporal brightenings occur in the S-shaped filament in the enhanced network southwest of the AR complex, as well as in, and adjacent to, a filament channel extending from the S-shaped filament to the west. The existence of magnetic connections to these quite remote areas, which are marked in Figure 8 below, is thus indicated. Part of the connections are also seen in the PFSS extrapolation (Figure 3). Later, these remote areas show the rise of material, associated with brightenings and dimmings, in close relation to the main eruptive flare.

The chain of coupled events can be traced back at least to the activation of the large loop system containing filament material (dark in He II 304 Å) south of AR 11515, which commenced at \sim 05 UT, i.e. with the first jet ejected from the NEF area. AIA 304 and 193 Å images show that the jet is ejected into a

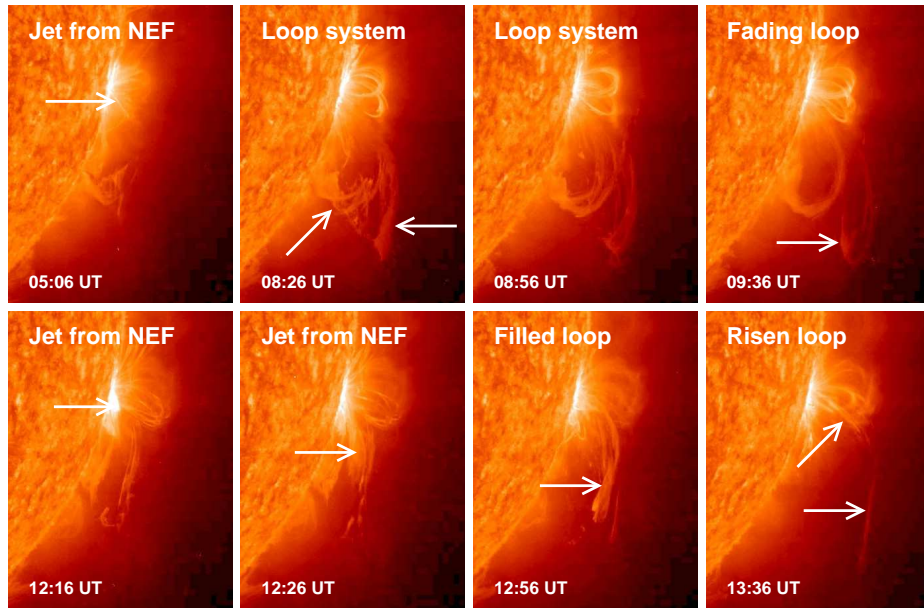


Figure 7. EUVI-B 304 Å snapshots of the two confined loop and filament activations south of AR 11515 during 05–10:30 UT (top row) and 12:10–13:40 UT (bottom row), both before the eruptive flare. The rise of three loops south of the AR complex, all containing filament material, is seen following the ejection of a jet from the NEF at ~ 05 and 12:10 UT, respectively. The loops fade subsequently, mostly due to the draining of the cool material (the lower loop seen in panel (d) fades by the time of panels (e)–(f)).

large loop connecting the area of the LS and the negative polarity of AR 11515 and extending to about S35. The loop then expands in the south, east, and west directions, reaching $\sim S50$ by 10:30 UT, when it fades in the 304 Å images. A second, somewhat smaller loop, lying below the first one in the EUVI-B limb view and seen only in the 304 Å band, also starts to expand. These loops are relatively faint in the AIA images, where they are most clear in animated image sequences, but are clearly seen in the limb view of STEREO Behind. The EUVI-B images (Figure 7(a–d)) show the rise of a multithreaded loop, filled with He II-emitting plasma and apparently rooted in the AR complex and about 10° farther south, from 05 UT onwards. The threads in the southern part, which in part obviously belong to the smaller loop in the AIA images, show indications of helical structure and undergo various changes until the flux is organized in two loops, which reach maximum heights of ~ 0.15 and $\sim 0.25 R_\odot$ during 9–10 UT. Both loops then fade at these positions, the upper one by $\approx 10:20$ UT, the lower one about two hours later. This filament activation appears to be confined.

Of the further jet emissions in AR 11515, the southward ones from the NEF area commencing at about 10:50 and 12:10 UT trigger similar effects in the AR complex, which eventually evolve into the eruptive flare. The initially slow expansion of a similar southward-oriented loop (lying inside the previously expanded one in the AIA images) is triggered by the first jet and accelerated by the second. This loop shows a stronger westward expansion. Its western leg

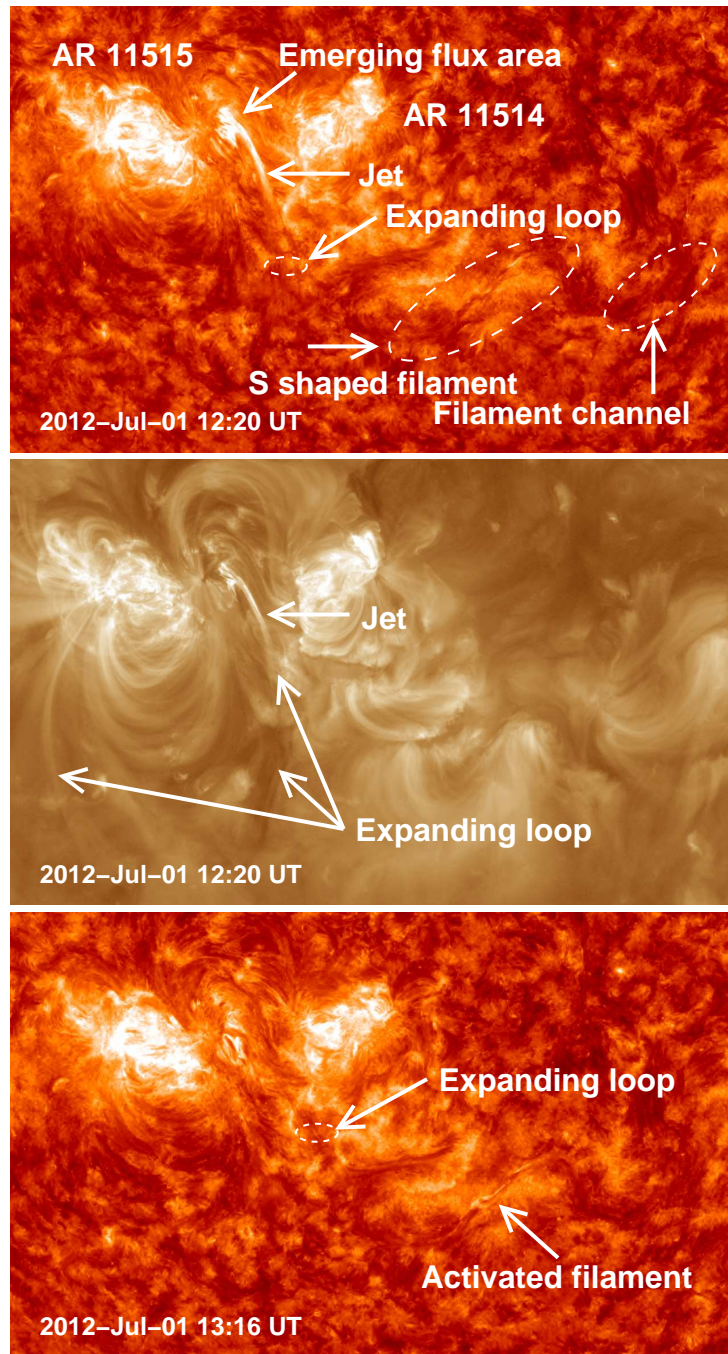


Figure 8. AIA 304 and 193 Å snapshots of the second activation, that directly leads to the eruptive flare. Several thin threads of absorbing (filament) material in the expanding loop system are enclosed by small ellipses in the 304 Å images. At 193 Å the legs of the expanding loop system are clearly seen in the still image, while the top part can be discerned against the structured background only in animated image sequences. Two large ellipses outline the positions of the S-shaped filament and the filament channel westward of it, which become involved in the eruption.

sweeps over the S-shaped filament in the enhanced network southwest of the AR complex, reaching it at 13:12 UT, simultaneously with the onset of brightenings in the filament (Figure 8). The loop fades in the AIA 304 Å images by 13:42 UT, when it crosses over the filament roughly in the middle. The jet at 12:10 UT and subsequent loop expansion are also imaged by EUVI-B (Figure 7(e-h)). These 304 Å images show that the jet is ejected into the height range of the previously activated loop ($\sim 0.15 R_{\odot}$). The He II-emitting material forms a new multi-threaded loop, which quickly rises to $\sim 0.4 R_{\odot}$, but stops at this height. The material then slides northward, back to the surface and the loop fades, disappearing at $\approx 14:00$ UT; this activity apparently also remains confined. Nevertheless, the flux above the legs of this loop, which become nearly vertical, from $\sim 25^{\circ}$ to the surface at the time of the jet ejection to $\sim 70^{\circ}$ at the fading, must be substantially disturbed. Primarily the western leg, running under the middle field lobe of the AR complex, must be seen in the EUVI-B 304 Å data, because this leg is much clearer than the eastern leg in the corresponding AIA data. The loops seen above the AR complex in the EUVI-B 304 Å images extend within the area of the two ARs, but do not pass over the expanding loop (Figure 8); therefore, they are not lifted.

The corresponding EUVI-B 195 Å images show the rise of diffuse, multiple loop structures south of the AR complex from ~ 11 UT, also stalled at $\sim 0.4 R_{\odot}$ by ~ 14 UT. These are not displayed here, since they show the rising structures only very faintly.

The second activation of the loop system south of AR 11515 and its strong westward expansion trigger several brightenings in the S-shaped filament in the enhanced network southwest of AR 11514, and fast motions of brightened material along the axis of the filament. At least one thread detaches and moves away from the filament in a perpendicular (southwest) direction, followed by a pair of moderately intense ribbons developing on either side of the filament from 13:48 UT onward (these can still be seen 90 min later in Figure 10(a)). Clearly, there is an eruption of flux in the channel that includes this filament, but is mostly lying above the filament. A partial eruption of the S-shaped filament is also obvious from its reduced darkness in the $H\alpha$ images. The AIA 193 Å images reveal more clearly that the corona above the S-shaped filament strongly expands southward as the ribbons to the sides of the filament spread, suggestive of the opening of the field in this area, which dims subsequently.

Related activities also occur in and adjacent to the filament channel extending westward from the S-shaped filament. These include a very localized ejection of bright material near its western end during 12:45–13 UT, precisely at the location of a brightening caused by the earlier activation during 03:40–04 UT, and a southward-directed eruption from this filament channel essentially simultaneous with the development of the ribbons of the S-shaped filament. This eruption leads to a deep and extended dimming. The locations of these developments in the area of enhanced network are identified in Figures 8 and 10.

4.2. The eruptive flare

Although the pre-eruptive and eruptive activity extends over the whole AR complex and the large neighboring area of enhanced network to the southwest,

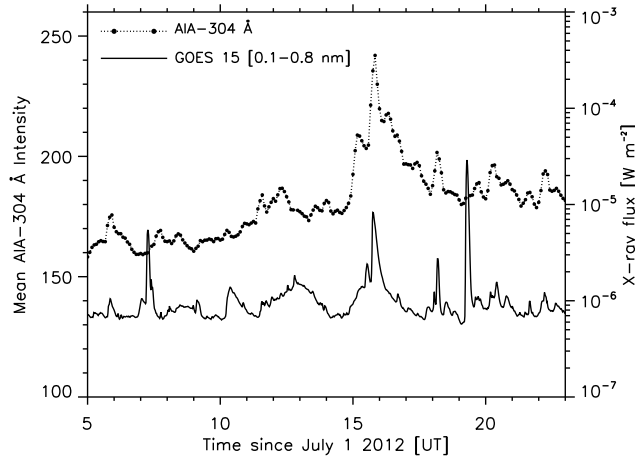


Figure 9. Temporal evolution of the mean AIA 304 Å intensity (dotted line with filled circles) in the active region and the GOES 15 soft X-ray flux in the 0.1–0.8 nm band (solid line). Both the C5.4 flare at 07:11 UT and the M2.8 flare at 19:11 UT occurred in AR 11513.

the core of the eruption clearly is the PIL between ARs 11514 and 11515. The bright ribbons begin to form near the ends of this PIL, where they enclose the initial dimmings, and the ribbons and flare loop arcade extend along this PIL. Subsequently, extended dimmings, interspersed with small-scale brightenings, form in other places, indicating that the overlying flux had a complex topology and that the erupting flux reconnected with overlying flux, exchanging the footpoints.

The ribbons of the eruptive C8.3 flare, which peaks at 15:45 UT (Figure 9), begin to form in the positive flux ahead and northwest of the LS in AR 11515 at 14:30 UT and about 8 minutes later at the eastern edge of the most eastern enhanced network cell south of AR 11514 (Figure 10(a)). This onset time coincides with the time the ribbons at the activated S-shaped filament in the enhanced network have reached their maximum separation. Thus, there is a continuous sequence of events, starting with jet ejections at the NEF, continuing into the activation and rise of a large loop that runs under the middle lobe of the AR complex and at the same time sweeping over the area of enhanced network. This is followed by the partial eruption of the S-shaped filament and the adjacent filament channel in the enhanced network, and finally by the destabilization of the flux in the middle lobe of the AR complex. The arc-shaped initial section of the ribbon in the positive-flux area encloses the initial dimming area, which includes about one-third of the LS. On the other side, the initial dimming extends over half of the network cell bounded by the initial ribbon. These are the best candidates for the footpoint regions of the destabilized flux. They are marked in Figure 10(a).

The erupting flux can be discerned only partly and is extremely difficult to visualize, since it does not contain any cool material. Animated images of AIA 193, 211, and 335 Å display a very faint and diffuse loop that propagates

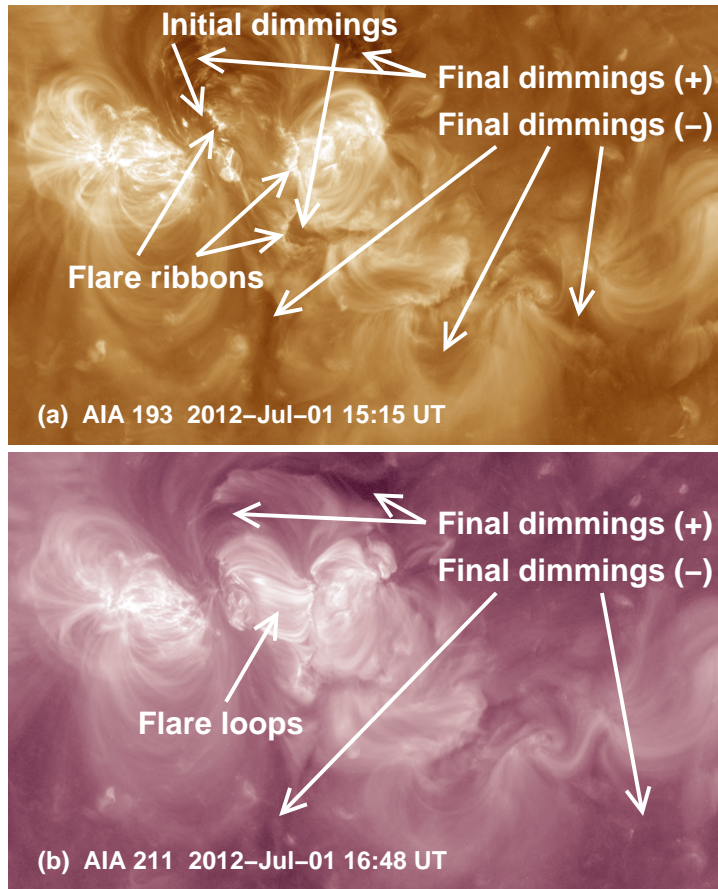


Figure 10. AIA images of the early (top, 193 Å) and late (bottom, 211 Å) evolution of the eruptive C8.3 flare. The magnetic polarity of the dimming areas is indicated.

westward from the middle field lobe of the AR complex, up to $\sim 20^\circ$ west from the PIL, during 14:15–15:15 UT. The loop appears to be rooted in or near the initial positive flare ribbon, i.e. in or near the LS. In the southward direction it cannot be traced beyond the edge of AR 11514 against the complex and changing background. This is consistent with the dimming at the initial negative flare ribbon being its southern footpoint. The two initial dimmings deepen synchronously with the westward motion of the loop. The detection in the 193, 211, and 335 Å bands, and the non-detection in the 94 and 131 Å bands, indicate a temperature in the range $1.5 \text{ MK} \lesssim T < 7 \text{ MK}$. The structure appears to be similar to the hot channel detected in other events, mostly above the limb (e.g., Zhang, Cheng, and Ding, 2012), with the lower temperature here corresponding to the moderate intensity of the flare. The hot channel is assumed to show the erupting flux rope.

Within the next half hour, the ribbons quickly extend along the PIL, especially the ribbon in the weaker negative flux, which then covers the whole north-south

extent of negative flux at the trailing side of the enhanced network and AR 11514 (this is indicated in Figure 10(a)). The other ribbon extends into positive network north of the LS and propagates toward the center of the LS. Simultaneously, several dimming areas begin to develop. These include an extended area of positive network north of the unstable middle flux lobe (where a prominent set of interconnecting loops existed before the eruption and was strongly disturbed), the erupting S-shaped filament and adjacent filament channel in the enhanced network southwest of AR 11514, and a substantial area of negative network extending south from the initial negative ribbon (Figure 10(b)). These dimming areas last for several hours. The three southern ones formed in the first place during the pre-eruption activities (rise of the large loops south of AR 11515 and rise of flux above the S-shaped filament and adjacent filament channel southwest of AR 11514 from 13:12 UT onward), but extend farther in the course of the eruptive flare. They indicate that the erupting flux reconnects and exchanges footpoints with originally overlying flux rooted in at least some of the dimming areas.

This is supported by the EUVI-B 195 Å images of the eruption, which show a loop expanding radially and southward above the AR complex from about 14:40 UT onward (then at a height of $\sim 0.3 R_{\odot}$). The loop appears to be rooted in the AR complex and up to 20° south of it (the precise location being masked by foreground and background loops). This is consistent with the dimmings in the positive network regions southwest and south of the AR complex. Since the loop in the EUVI-B 195 Å images is too faint for a visualization in still images, even when using difference images, Figure 11 shows a COR1-B difference image of the CME at an early stage, when it still expands in the same latitude range as the loop imaged by EUVI-B at 195 Å.

The direction of the flux overlying the middle field lobe of the AR complex, implied by the location of the dimmings in AIA images, is roughly from north-east to south-west, i.e. rather close to the direction of the flux in the lobe, especially if the sheared loops in the lobe are considered. This is different from the configuration of the breakout model for eruptions.

The arcade of flare loops forms at the section of the PIL between the two ARs, supporting the view that the destabilization of sheared flux in the middle lobe of the AR complex caused the eruption. The usual evolution from considerably sheared first flare loops to more potential ones later on can be seen (Figures 10(b) and 12(b-d)). The first flare loops form after 14:38 UT in AIA 94 and 131 Å images ($T \sim 7\text{--}11$ MK).

A fast, southward-propagating CME appears in the LASCO/C2 field of view at 15:35 UT. A second-order fit yields a velocity of 800 km s^{-1} at the heliocentric distance of $3 R_{\odot}$. The propagation direction is southwestward in the field of view of COR1-B (Figure 11), where the CME appears at 15:00 UT.

The C2.4 flare peaking at 15:32 UT, i.e. during the rise of the flare in the AR complex studied here, is a compact and confined, likely sympathetic flare in AR 11513.

4.3. Superimposed confined flaring activity

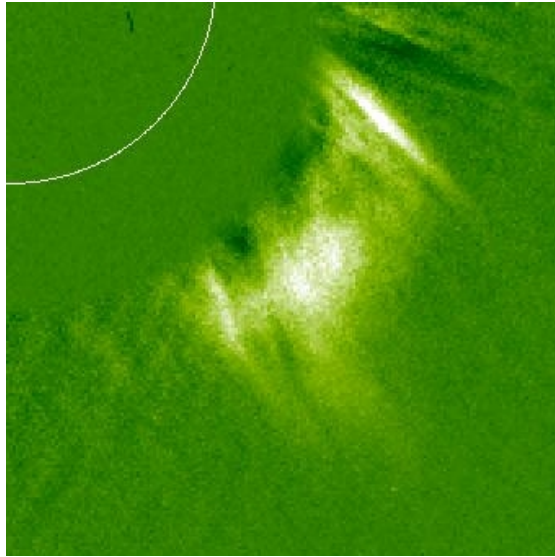


Figure 11. COR1-B running-difference image at 15:30 UT showing the considerable southward angular extent of the erupting flux, consistent with it being rooted in the negative-polarity dimming areas south of the AR complex, which are marked in Figure 10.

Two confined flares, one in AR 11515, the other in AR 11514, are closely related to the eruptive flare. Both occur under the closed, main field lobe of their bipolar host AR. The one in AR 11515 marks the peak of the emission of the C8.3 flare at 15:45 UT, i.e., is brighter than the eruptive flare. However, the confined flare is clearly a separate event, occurring in a different lobe of flux, where it remains compact and confined, and developing on a much shorter timescale. It is located at the PIL formed by the westward tongue of negative flux in the middle of the AR. In the AIA 131 Å band, it develops only from 15:37 UT onward, one hour after the onset of the eruptive flare. The other confined flare occurs within 5–10 minutes from the first at the northern end of the internal PIL in AR 11514. These confined flares are most sharply imaged in the 171 Å band, as shown in Figure 12; they are of course more prominent, but more diffuse, in the “hot” AIA bands, up to 131 Å. Both may be triggered by changes in their overlying flux caused by the rise of the flux in the eruptive flare. In particular, material is seen rising from a position very near the second flare immediately before its onset.

A third confined flare, of X-ray class C2.7, occurs in the NEF during the decay of the eruptive flare, i.e. under the flare loop arcade (see also Figure 12). Its loops are oriented north-south, as is part of the field rooted in the newly emerged flux ahead of the LS (Section 3). A detailed inspection of the 171 Å data suggests that the NEF brightens due to reconnection with loops rooted under the flare loop arcade, which show brief brightenings and changes in shape (see the 171 Å data in the animation accompanying Figures 1 and 2.) Most likely, the continuously rising NEF pushes against the re-closed field of the middle lobe

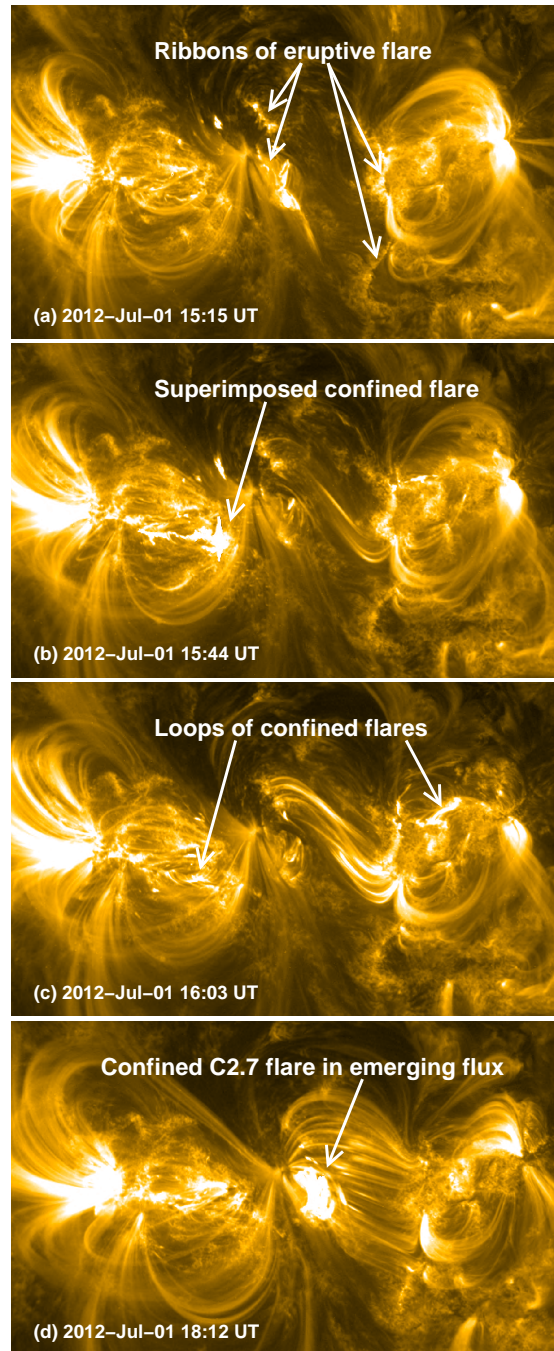


Figure 12. AIA 171 Å images of the additional confined flares. (a) Early phase of the eruptive flare, before the confined flares; (b) peak emission of the combined eruptive and first additional confined flares; (c) loops of the two confined flares in AR 11515 and AR 11514 after their peak times; (d) peak emission of the confined C2.7 flare in the NEF under the arcade of the eruptive flare.

in the AR complex, and the temporal association with the decay phase of the eruptive flare is accidental.

5. Discussion: initiation of the eruption

The eruption occurs at the PIL between ARs 11514 and 11515, under the middle lobe of a three-lobe magnetic configuration, where the field is considerably sheared and a filament channel is forming. Moreover, new flux is emerging under the lobe near its edge. The amount of new flux emerged by the time of the eruption is only $\sim 40\%$ of the flux in the middle lobe. The observations are inconclusive with regard to the question whether a flux rope was formed (or is forming) above the PIL, or whether the flux has the structure of a sheared arcade.

Both basic possibilities for the triggering of eruptions appear consistent with the data: the equilibrium of sheared (current-carrying) flux can be destroyed either by an increase of the current beyond the limit of stability, or by a weakening of the external flux (rooted in photospheric sources other than the sheared flux) by a sufficient amount, such that it can no longer stabilize the upward-directed Lorentz self-force of the given current. The first option is supported by the flow toward the PIL from the trailing side of AR 11514. This transports negative flux to the PIL, some of which cancels there with positive network flux, increasing the shear and current above the PIL. However, by the amount of flux involved (around 1.5×10^{18} Mx, ≈ 450 times smaller than the amount of emerging flux), this is a very weak effect compared to the multitude of other pre-flare activities that affect the large-scale field structure of the AR complex. Therefore, we consider such “internal triggering” at the PIL to be *far* less likely than an external triggering by changes of the ambient field.

A classical model for external triggering in a quadrupolar source region is the breakout model (Lynch *et al.*, 2008; Karpen, Antiochos, and DeVore, 2012). This model relies on the weakening of the ambient flux in the middle lobe by reconnection with an overlying fourth lobe of essentially opposite direction. We do not find signatures that such a lobe exists and contains a sufficient amount of flux. The PFSS extrapolation is inconclusive with regard to the existence and direction of such a field lobe, but indicates that not much flux could be contained if it exists. The dimmings developing in association with the eruption indicate that the overlying flux is directed relative to the middle field lobe at an angle smaller than 90° , basically opposite to the model. Therefore, it is unlikely that the breakout model can explain the onset of the eruption.

The event yields many strong indications that the episode of newly emerging flux under the middle flux lobe triggers interactions with the large-scale field in the AR complex, which lead to an upward expansion of the middle lobe, weakening its stabilizing downward tension force. The most likely scenario in our opinion is that the rise of the large loop system south of AR 11515, which is rooted near the area of NEF and the LS and initially runs at a low elevation, i.e. essentially under the middle flux lobe, lifts the lobe quite strongly (see, in particular, Figure 7(f–h)). Additionally, the expansion of the loop system

probably triggers the eruption of the S-shaped filament in the enhanced network southwest of AR 11514, and of the filament channel extending westward from the filament. These secondary eruptions perturb the large-scale field structure in the AR complex, as is obvious from the development of dimmings, and very likely have a share in lifting the middle flux lobe. This is indicated by their close temporal association with the main eruption, which commences while they are in progress. Each of the relevant pre-eruption activities commences with, or is amplified by, a jet emission from the NEF. The jets are emitted *into* the large loop system south of AR 11515, which thus has become magnetically connected with the NEF through reconnection. The loop system must carry currents already before the eruption, since the PFSS extrapolation does not yield any low-lying field lines at the location of the loop system. There is no doubt that the currents, and consequently the equilibrium of the loop system, are strongly perturbed when the loop system reconnects with the NEF.

Thus, we trace the origin of the eruption to the NEF, one of the standard options for eruption triggering (e.g., Schrijver, 2009). The particular trigger mechanism in the present event, however, is partly different from the mechanisms considered so far. Both observations (Feynman and Martin, 1995) and modeling find the triggering of eruptions by emerging flux to be most efficient when the new flux is directed oppositely to the existing flux, such that reconnection commences easily. This is true for emergence both near the PIL and near the edge of the arcade field overlying the PIL, although the latter case was found to be restricted in the range of distances to the PIL (Xu, Fang, and Chen, 2008). The reconnection destabilizes a pre-existing flux rope (Chen and Shibata, 2000; Xu, Chen, and Fang, 2005) or transforms the inner part of a pre-existing sheared arcade into an unstable flux rope (Kusano *et al.*, 2012; Kaneko and Yokoyama, 2014). Alternatively, the emerging flux itself forms a flux rope, and the reconnection of this flux rope with a pre-existing arcade is essential for the removal of the rope's own stabilizing envelope, such that the rope will erupt (Archontis and Török, 2008; Archontis and Hood, 2012; Leake, Linton, and Antiochos, 2014). None of these mechanisms appears to be at work in the eruption studied here. The dominant orientation of the NEF is between westward and southward, not much different from the orientation of the pre-existing flux in the middle field lobe, so that the mechanisms based on the occurrence of reconnection with antiparallel or nearly antiparallel field, elaborated in the above articles, are not applicable. Additionally, the amount of flux emerged by the time of the eruption is considerably smaller than the pre-existing flux, clearly insufficient for the alternative arcade compression mechanism studied by Kaneko and Yokoyama (2014).

Our suggestion of destabilization by lifting the overlying flux bears some similarity to the findings in Wang and Sheeley (1999). These authors used a superposition of potential (vacuum) fields to model the effect of new flux emergence and obtained a lifting or sideways deflection of flux overlying filaments that erupted. This is conceptually different from the lifting of the middle flux lobe by the rise of the activated loop system in our suggested scenario, which must be driven by Lorentz forces, but has a similar effect on the stability of the sheared flux in the filament channel.

The NEF in the present event does reconnect with overlying, pre-existing flux, but this flux is not part of the later erupting middle lobe of the quadrupolar AR

complex, but rather part of a side lobe (AR 11515). This flux, seen as a large loop system south of AR 11515, and rooted at both ends in this AR, runs under one side of the middle lobe. Its direction is not much different from the field direction in the middle lobe, and no signs of reconnection with the middle lobe (any brightenings other than the jet ejection from the NEF into the loop system) are seen in either AIA or EUVI-B images. This indicates that the rise of the loop system and the consequent lifting of the flux in the middle lobe is the dominant effect that destabilizes the lobe.

Although the magnetic topology of the eruption may be a relatively rare occurrence, it need not be a singular case. Configurations with both interconnecting loops to a preceding active region and internal loops in an active region emerging from the leading sunspot are common. New flux is often seen to emerge in the vicinity of existing flux concentrations.

The observations do not yield a conclusive hint on whether or not a flux rope already exists by the time the middle lobe is lifted. If none existed before, a rope must form in response to the lifting, because otherwise there would be no eruption—there is no ideal MHD instability of a sheared arcade (e.g., Roumeliotis, Sturrock, and Antiochos, 1994; Mikic and Linker, 1994; Amari *et al.*, 1996). One can expect that the lifting of a sufficiently sheared arcade by external forces induces Lorentz forces in the lifted flux that point toward the middle of the arcade and lead to a horizontal constriction that steepens a vertical current sheet in the center of the arcade. This is similar to the enforced rise of an arcade over an unstable flux rope, which leads to a constriction of the flux under the rope, current sheet steepening, and eventually to flare reconnection. Here the reconnection would form a flux rope if none existed before and then continue in the standard manner of flare reconnection, amplified by the eruption of the formed rope.

Following perturbations by the NEF, part of the loop system running south of AR 11515 and under the middle lobe begins to rise. However, all loops find a new equilibrium height (Figure 7), whereas the sheared flux under the middle lobe erupts into a CME. This difference is likely related to a difference in the nature of the two structure’s force-free equilibria. We suggest the following explanation. The current in the sheared flux rooted near the PIL is likely stabilized by the overlying flux of the middle lobe rooted to a large part away from the PIL at the edges of the adjacent ARs. This is the classic force-free equilibrium of flux carrying a net current in external, essentially potential flux, as proposed by van Tend and Kuperus (1978) and elaborated by Titov and Démoulin (1999). This equilibrium admits an instability (torus instability) when the sheared flux transforms, at least partly, into a flux rope above the PIL (van Tend and Kuperus, 1978; Kliem and Török, 2006). It is difficult to see how such an equilibrium could be established for the loop system south of AR 11515, because there is hardly any significant amount of flux rooted in the area south of the loop system (Figure 2). Therefore, the equilibrium of the loop system, which also carries electric currents (as argued above), is likely provided by a return current such that the net current along the loop system vanishes. Such force-free equilibria exist for arcades and flux ropes; the flux rope can have the shape of a loop. While the arcades are stable, flux ropes may admit an instability of the helical kink mode. However,

the existence of instability for such flux ropes is not yet clarified (Török and Kliem, 2003; Aulanier, Démoulin, and Grappin, 2005). If instability occurs, a minimum twist of about one field line turn is required. The EUV images of the loop system do not provide any evidence supporting this substantial requirement (see Figures 2 and 8). Therefore, the loop system is probably in a very stable force-free equilibrium. Its reconnection with the NEF must change its currents, such that it acquires a new equilibrium at a higher position without erupting.

6. Conclusions

The present investigation of an eruptive C8.3 flare and fast CME on July 1, 2012 in the AR complex consisting of ARs 11514 and 11515 reveals a new scenario of eruption triggered by emerging flux. The emergence occurs under the middle flux lobe of a quadrupolar configuration (between the two ARs) far away from the PIL. Most of the emerging flux is roughly aligned with the arcade-like large-scale flux in this lobe, not favorable for reconnection with it. Moreover, the amount of emerging flux remains moderate, reaching only $\sim 40\%$ of the pre-existing flux of the lobe by the time of the eruption. A relatively particular circumstance is given by the fact that a large loop system of the trailing AR 11515, rooted in the leading spot of the region, passes under the middle lobe, which is also largely rooted in this spot. The new flux emerges in front of the spot, under the loop system. It reconnects with the loop system, ejecting a series of jets into the loop system, which then rises considerably (changing its inclination to the surface from 25° to 70°) but does not erupt by itself. The rise of the loop system lifts the flux of the middle lobe, reducing its stabilizing downward-tension. This triggers the eruption of the strongly sheared flux in the center of the lobe.

The eruption is also noteworthy for its location. The structure of the magnetogram would hardly suggest that an eruption occurs in the extended area of very weak field between the two ARs, one of them already decaying. Instead, one would expect an eruption to occur in the complex field of the developing AR, which also harbors the emergence of new flux in the immediate vicinity of its leading spot (where an eruption, analyzed in Lo14, indeed occurs 19 hours later). However, the chromospheric and coronal structures indicate magnetic shear at the PIL between the ARs, correctly pointing at the site of the eruption studied here.

Acknowledgements We gratefully acknowledge constructive comments by the referee, which were helpful in improving the clarity of this paper. R.E.L. is grateful for the financial assistance from the German Science Foundation (DFG) under grant DE 787/3-1 and the European Commission's FP7 Capacities Programme under the Grant Agreement number 312495. G.C. and B.K. acknowledge support by the NSF under Grant No. 1249270. B.K. also acknowledges support by the DFG. HMI data are courtesy of NASA/SDO and the HMI science team. They are provided by the Joint Science Operations Center – Science Data Processing at Stanford University. EUVI-B and COR1-B images are supplied courtesy of the STEREO Sun Earth Connection Coronal and Heliospheric Investigation (SECCHI) team. This work utilizes data obtained by the Global Oscillation Network Group (GONG) Program, managed by the National Solar Observatory, which is operated by AURA, Inc. under a cooperative agreement with the National Science Foundation. The data were acquired by instruments operated by the Big Bear Solar Observatory, High Altitude Observatory, Learmonth Solar Observatory,

Udaipur Solar Observatory, Instituto de Astrofísica de Canarias, and Cerro Tololo Interamerican Observatory. We have used the SOHO/LASCO CME catalog, generated and maintained at the CDAW Data Center by NASA and The Catholic University of America in cooperation with the Naval Research Laboratory. SOHO is a project of international cooperation between ESA and NASA.

References

- Amari, T., Luciani, J.F., Aly, J.J., Tagger, M.: 1996, Plasmoid formation in a single sheared arcade and application to coronal mass ejections. *Astron. Astrophys.* **306**, 913. ADS.
- Amari, T., Luciani, J.F., Aly, J.J., Mikic, Z., Linker, J.: 2003, Coronal Mass Ejection: Initiation, Magnetic Helicity, and Flux Ropes. II. Turbulent Diffusion-driven Evolution. *Astrophys. J.* **595**, 1231. DOI. ADS.
- Amari, T., Aly, J.-J., Luciani, J.-F., Mikic, Z., Linker, J.: 2011, Coronal Mass Ejection Initiation by Converging Photospheric Flows: Toward a Realistic Model. *Astrophys. J. Lett.* **742**, L27. DOI. ADS.
- Archontis, V., Hood, A.W.: 2010, Flux emergence and coronal eruption. *Astron. Astrophys.* **514**, A56. DOI. ADS.
- Archontis, V., Hood, A.W.: 2012, Magnetic flux emergence: a precursor of solar plasma expulsion. *Astron. Astrophys.* **537**, A62. DOI. ADS.
- Archontis, V., Török, T.: 2008, Eruption of magnetic flux ropes during flux emergence. *Astron. Astrophys.* **492**, L35. DOI. ADS.
- Aulanier, G., Démoulin, P., Grappin, R.: 2005, Equilibrium and observational properties of line-tied twisted flux tubes. *Astron. Astrophys.* **430**, 1067. DOI. ADS.
- Aulanier, G., Török, T., Démoulin, P., DeLuca, E.E.: 2010, Formation of Torus-Unstable Flux Ropes and Electric Currents in Erupting Sigmoids. *Astrophys. J.* **708**, 314. DOI. ADS.
- Burtseva, O., Petrie, G.: 2013, Magnetic Flux Changes and Cancellation Associated with X-Class and M-Class Flares. *Solar Phys.* **283**, 429. DOI. ADS.
- Chen, P.F., Shibata, K.: 2000, An Emerging Flux Trigger Mechanism for Coronal Mass Ejections. *Astrophys. J.* **545**, 524. DOI. ADS.
- Démoulin, P., van Driel-Gesztelyi, L., Schmieder, B., Hemoux, J.C., Csepura, G., Hagyard, M.J.: 1993, Evidence for magnetic reconnection in solar flares. *Astron. Astrophys.* **271**, 292. ADS.
- Feynman, J., Martin, S.F.: 1995, The initiation of coronal mass ejections by newly emerging magnetic flux. *J. Geophys. Res.* **100**, 3355. DOI. ADS.
- Forbes, T.G., Priest, E.R.: 1995, Photospheric Magnetic Field Evolution and Eruptive Flares. *Astrophys. J.* **446**, 377. DOI. ADS.
- Gibson, S.E., Fan, Y.: 2006, The Partial Expulsion of a Magnetic Flux Rope. *Astrophys. J. Lett.* **637**, L65. DOI. ADS.
- Green, L.M., Kliem, B., Wallace, A.J.: 2011, Photospheric flux cancellation and associated flux rope formation and eruption. *Astron. Astrophys.* **526**, A2. DOI. ADS.
- Hagyard, M.J., Venkatakrishnan, P., Smith, J.B. Jr.: 1990, Nonpotential magnetic fields at sites of gamma-ray flares. *Astrophys. J. Suppl.* **73**, 159. DOI. ADS.
- Harvey, J.W., Hill, F., Hubbard, R.P., Kennedy, J.R., Leibacher, J.W., Pintar, J.A., Gilman, P.A., Noyes, R.W., Title, A.M., Toomre, J., Ulrich, R.K., Bhatnagar, A., Kennewell, J.A., Marquette, W., Patron, J., Saa, O., Yasukawa, E.: 1996, The Global Oscillation Network Group (GONG) Project. *Science* **272**, 1284. DOI. ADS.
- Harvey, J.W., Bolding, J., Clark, R., Hauth, D., Hill, F., Kroll, R., Luis, G., Mills, N., Purdy, T., Henney, C., Holland, D., Winter, J.: 2011, Full-disk Solar H-alpha Images From GONG. In: *AAS/Solar Physics Division Abstracts #42*, 1745. ADS.
- Howard, R.A., Moses, J.D., Vourlidas, A., Newmark, J.S., Socker, D.G., Plunkett, S.P., Korendyke, C.M., Cook, J.W., Hurley, A., Davila, J.M., Thompson, W.T., St Cyr, O.C., Mentzell, E., Mehalick, K., Lemen, J.R., Wuelser, J.P., Duncan, D.W., Tarbell, T.D., Wolfson, C.J., Moore, A., Harrison, R.A., Waltham, N.R., Lang, J., Davis, C.J., Eyles, C.J., Mapson-Menard, H., Simnett, G.M., Halain, J.P., Defise, J.M., Mazy, E., Rochus, P., Mercier, R., Ravet, M.F., Delmotte, F., Auchere, F., Delaboudiniere, J.P., Bothmer, V., Deutsch, W., Wang, D., Rich, N., Cooper, S., Stephens, V., Maahs, G., Baugh, R., McMullin, D., Carter, T.: 2008, Sun Earth Connection Coronal and Heliospheric Investigation (SECCHI). *Space Sci. Rev.* **136**, 67. DOI. ADS.

- Kaneko, T., Yokoyama, T.: 2014, Simulation Study of Solar Plasma Eruptions Caused by Interactions between Emerging Flux and Coronal Arcade Fields. *Astrophys. J.* **796**, 44. DOI. ADS.
- Karpen, J.T., Antiochos, S.K., DeVore, C.R.: 2012, The Mechanisms for the Onset and Explosive Eruption of Coronal Mass Ejections and Eruptive Flares. *Astrophys. J.* **760**, 81. DOI. ADS.
- Kliem, B., Török, T.: 2006, Torus Instability. *Phys. Rev. Lett.* **96**(25), 255002. DOI. ADS.
- Kusano, K., Bamba, Y., Yamamoto, T.T., Iida, Y., Toriumi, S., Asai, A.: 2012, Magnetic Field Structures Triggering Solar Flares and Coronal Mass Ejections. *Astrophys. J.* **760**, 31. DOI. ADS.
- Leake, J.E., Linton, M.G., Antiochos, S.K.: 2014, Simulations of Emerging Magnetic Flux. II. The Formation of Unstable Coronal Flux Ropes and the Initiation of Coronal Mass Ejections. *Astrophys. J.* **787**, 46. DOI. ADS.
- Lemen, J.R., Title, A.M., Akin, D.J., Boerner, P.F., Chou, C., Drake, J.F., Duncan, D.W., Edwards, C.G., Friedlaender, F.M., Heyman, G.F., Hurlburt, N.E., Katz, N.L., Kushner, G.D., Levay, M., Lindgren, R.W., Mathur, D.P., McFeaters, E.L., Mitchell, S., Rehse, R.A., Schrijver, C.J., Springer, L.A., Stern, R.A., Tarbell, T.D., Wuelser, J.-P., Wolfson, C.J., Yanari, C., Bookbinder, J.A., Cheimets, P.N., Caldwell, D., Deluca, E.E., Gates, R., Golub, L., Park, S., Podgorski, W.A., Bush, R.L., Scherrer, P.H., Gumm, M.A., Smith, P., Aufer, G., Jerram, P., Pool, P., Souffi, R., Windt, D.L., Beardsley, S., Clapp, M., Lang, J., Waltham, N.: 2012, The Atmospheric Imaging Assembly (AIA) on the Solar Dynamics Observatory (SDO). *Solar Phys.* **275**, 17. DOI. ADS.
- Li, H., Sakurai, T., Ichimoto, K., Ueno, S.: 2000, Magnetic Field Evolution Leading to Solar Flares I. Cases with Low Magnetic Shear and Flux Emergence. *Pub. Astron. Soc. Japan* **52**, 465. ADS.
- Lin, J., Forbes, T.G.: 2000, Effects of reconnection on the coronal mass ejection process. *J. Geophys. Res.* **105**, 2375. DOI. ADS.
- Lin, J., Forbes, T.G., Isenberg, P.A.: 2001, Prominence eruptions and coronal mass ejections triggered by newly emerging flux. *J. Geophys. Res.* **106**, 25053. DOI. ADS.
- Lites, B.W.: 2005, Magnetic Flux Ropes in the Solar Photosphere: The Vector Magnetic Field under Active Region Filaments. *Astrophys. J.* **622**, 1275. DOI. ADS.
- Livi, S.H.B., Martin, S., Wang, H., Ai, G.: 1989, The association of flares to cancelling magnetic features on the sun. *Solar Phys.* **121**, 197. DOI. ADS.
- Louis, R.E., Puschmann, K.G., Kliem, B., Balthasar, H., Denker, C.: 2014, Sunspot splitting triggering an eruptive flare. *Astron. Astrophys.* **562**, A110. DOI. ADS.
- Low, B.C.: 1996, Solar Activity and the Corona. *Solar Phys.* **167**, 217. DOI. ADS.
- Lynch, B.J., Antiochos, S.K., DeVore, C.R., Luhmann, J.G., Zurbuchen, T.H.: 2008, Topological Evolution of a Fast Magnetic Breakout CME in Three Dimensions. *Astrophys. J.* **683**, 1192. DOI. ADS.
- Mackay, D.H., van Ballegoijen, A.A.: 2006, Models of the Large-Scale Corona. I. Formation, Evolution, and Liftoff of Magnetic Flux Ropes. *Astrophys. J.* **641**, 577. DOI. ADS.
- Mackay, D.H., Karpen, J.T., Ballester, J.L., Schmieder, B., Aulanier, G.: 2010, Physics of Solar Prominences: II—Magnetic Structure and Dynamics. *Space Sci. Rev.* **151**, 333. DOI. ADS.
- Manchester, W. IV, Gombosi, T., DeZeeuw, D., Fan, Y.: 2004, Eruption of a Buoyantly Emerging Magnetic Flux Rope. *Astrophys. J.* **610**, 588. DOI. ADS.
- Martin, S.F.: 1998, Conditions for the Formation and Maintenance of Filaments (Invited Review). *Solar Phys.* **182**, 107. DOI. ADS.
- Martin, S.F., Dezso, L., Antalova, A., Kucera, A., Harvey, K.L.: 1982, Emerging magnetic flux, flares and filaments - FBS interval 16-23 June 1980. *Advances in Space Research* **2**, 39. DOI. ADS.
- Martres, M.-J., Michard, R., Soru-Iscovi, I., Tsap, T.T.: 1968, Étude de la localisation des éruptions dans la structure magnétique évolutive des régions actives solaires. *Solar Phys.* **5**, 187. DOI. ADS.
- Mikic, Z., Linker, J.A.: 1994, Disruption of coronal magnetic field arcades. *Astrophys. J.* **430**, 898. DOI. ADS.
- Pesnell, W.D., Thompson, B.J., Chamberlin, P.C.: 2012, The Solar Dynamics Observatory (SDO). *Solar Phys.* **275**, 3. DOI. ADS.
- Roumeliotis, G., Sturrock, P.A., Antiochos, S.K.: 1994, A Numerical Study of the Sudden Eruption of Sheared Magnetic Fields. *Astrophys. J.* **423**, 847. DOI. ADS.
- Rust, D.M.: 1972, Flares and Changing Magnetic Fields. *Solar Phys.* **25**, 141. DOI. ADS.

- Sakajiri, T., Brooks, D.H., Yamamoto, T., Shiota, D., Isobe, H., Akiyama, S., Ueno, S., Kitai, R., Shibata, K.: 2004, A Study of a Tiny Two-Ribbon Flare Driven by Emerging Flux. *Astrophys. J.* **616**, 578. DOI. ADS.
- Savcheva, A.S., Green, L.M., van Ballegoijen, A.A., DeLuca, E.E.: 2012, Photospheric Flux Cancellation and the Build-up of Sigmoidal Flux Ropes on the Sun. *Astrophys. J.* **759**, 105. DOI. ADS.
- Schou, J., Scherrer, P.H., Bush, R.I., Wachter, R., Couvidat, S., Rabello-Soares, M.C., Bogart, R.S., Hoeksema, J.T., Liu, Y., Duvall, T.L., Akin, D.J., Allard, B.A., Miles, J.W., Rairden, R., Shine, R.A., Tarbell, T.D., Title, A.M., Wolfson, C.J., Elmore, D.F., Norton, A.A., Tomczyk, S.: 2012, Design and Ground Calibration of the Helioseismic and Magnetic Imager (HMI) Instrument on the Solar Dynamics Observatory (SDO). *Solar Phys.* **275**, 229. DOI. ADS.
- Schrijver, C.J.: 2009, Driving major solar flares and eruptions: A review. *Advances in Space Research* **43**, 739. DOI. ADS.
- Schuck, P.W.: 2006, Tracking Magnetic Footpoints with the Magnetic Induction Equation. *Astrophys. J.* **646**, 1358. DOI. ADS.
- Sterling, A.C., Chifor, C., Mason, H.E., Moore, R.L., Young, P.R.: 2010, Evidence for magnetic flux cancellation leading to an ejective solar eruption observed by Hinode, TRACE, STEREO, and SoHO/MDI. *Astron. Astrophys.* **521**, A49. DOI. ADS.
- Sun, X., Hoeksema, J.T., Liu, Y., Wiegmann, T., Hayashi, K., Chen, Q., Thalmann, J.: 2012, Evolution of Magnetic Field and Energy in a Major Eruptive Active Region Based on SDO/HMI Observation. *Astrophys. J.* **748**, 77. DOI. ADS.
- Titov, V.S., Démoulin, P.: 1999, Basic topology of twisted magnetic configurations in solar flares. *Astron. Astrophys.* **351**, 707. ADS.
- Török, T., Kliem, B.: 2003, The evolution of twisting coronal magnetic flux tubes. *Astron. Astrophys.* **406**, 1043. DOI. ADS.
- van Ballegoijen, A.A., Martens, P.C.H.: 1989, Formation and eruption of solar prominences. *Astrophys. J.* **343**, 971. DOI. ADS.
- van Tend, W., Kuperus, M.: 1978, The development of coronal electric current systems in active regions and their relation to filaments and flares. *Solar Phys.* **59**, 115. DOI. ADS.
- Wang, H.: 2006, Rapid Changes of Photospheric Magnetic Fields around Flaring Magnetic Neutral Lines. *Astrophys. J.* **649**, 490. DOI. ADS.
- Wang, J., Shi, Z.: 1993, The flare-associated magnetic changes in an active region. II - Flux emergence and cancellation. *Solar Phys.* **143**, 119. DOI. ADS.
- Wang, Y.-M., Sheeley, N.R. Jr.: 1999, Filament Eruptions near Emerging Bipoles. *Astrophys. J. Lett.* **510**, L157. DOI. ADS.
- Xu, X.-Y., Chen, P.-F., Fang, C.: 2005, A Parametric Survey of the CME Triggering Process by Numerical Simulations. *Chin. J. Astron. Astrophys.* **5**, 636. DOI. ADS.
- Xu, X.-Y., Fang, C., Chen, P.-F.: 2008, A Statistical Study on the Filament Eruption Caused by New Emerging Flux. *Chin. Astron. Astrophys.* **32**, 56. DOI. ADS.
- Zhang, J., Cheng, X., Ding, M.-D.: 2012, Observation of an evolving magnetic flux rope before and during a solar eruption. *Nature Communications* **3**, 747. DOI. ADS.
- Zhao, X., Hoeksema, J.T.: 1995, Prediction of the interplanetary magnetic field strength. *J. Geophys. Res.* **100**, 19. DOI. ADS.